Video Article

Visualization and Quantification of the Cell-free Layer in Arterioles of the Rat Cremaster Muscle

Yan Cheng Ng[1,2], Liam K. Fisher[2], Veena Salim[2], Sangho Kim[1,2,3], Bumseok Namgung[2]

[1]NUS Graduate School for Integrative Sciences and Engineering, National University of Singapore

[2]Department of Biomedical Engineering, National University of Singapore

[3]Department of Surgery, National University of Singapore

Correspondence to: Bumseok Namgung at cienab@nus.edu.sg

URL: https://www.jove.com/video/54550
DOI: doi:10.3791/54550

Keywords: Biomedical Engineering, Issue 116, plasma layer, hemodynamics, microcirculation, cremaster muscle preparation, microvasculature, blood flow visualization

Date Published: 10/19/2016

Citation: Ng, Y.C., Fisher, L.K., Salim, V., Kim, S., Namgung, B. Visualization and Quantification of the Cell-free Layer in Arterioles of the Rat Cremaster Muscle. *J. Vis. Exp.* (116), e54550, doi:10.3791/54550 (2016).

Abstract

The cell-free layer is defined as the parietal plasma layer in the microvessel flow, which is devoid of red blood cells. The measurement of the *in vivo* cell-free layer width and its spatiotemporal variations can provide a comprehensive understanding of hemodynamics in microcirculation. In this study, we used an intravital microscopic system coupled with a high-speed video camera to quantify the cell-free layer widths in arterioles *in vivo*. The cremaster muscle of Sprague-Dawley rats was surgically exteriorized to visualize the blood flow. A custom-built imaging script was also developed to automate the image processing and analysis of the cell-free layer width. This approach enables the quantification of spatiotemporal variations more consistently than previous manual measurements. The accuracy of the measurement, however, partly depends on the use of a blue filter and the selection of an appropriate thresholding algorithm. Specifically, we evaluated the contrast and quality of images acquired with and without the use of a blue filter. In addition, we compared five different image histogram-based thresholding algorithms (Otsu, minimum, intermode, iterative selection, and fuzzy entropic thresholding) and illustrated the differences in their determination of the cell-free layer width.

Video Link

The video component of this article can be found at https://www.jove.com/video/54550/

Introduction

In vivo animal studies are instrumental to basic science for understanding human physiology and pathology. In particular, *in vivo* microhemodynamic studies can elucidate the potential impairment of microcirculatory functions altered by abnormal rheological conditions of blood. A number of previous microhemodynamic studies[1] have used the rat cremaster muscle model for visualizing microvascular blood flow. The cremaster muscle is a thin layer of striated muscle surrounding the testes. Thus, the blood flow in the muscle can be visualized with a trans-illumination microscope by means of surgical exposure. This enables us to acquire the *in vivo* blood flow images without the use of any fluorescence or contrast agents. In addition, the entire blood perfusion of the muscle network can be controlled by reducing the upstream blood flow with abdominal aorta occlusion[2]. Owing to these advantages, the cremaster muscle model has been widely used to investigate the formation of cell-free layer (CFL) in microvessels[1,3].

The CFL width is a prominent hemodynamic parameter in microcirculation, which has been of great interest for its important roles in regulating microcirculatory functions. The CFL is formed by the shear-induced transverse inward migration of red blood cells (RBCs) towards the flow center[4]. Consequently, this migration leads to the depletion of RBCs near the vessel walls, eventually resulting in a cell-free plasma layer. Accordingly, the parietal CFL naturally becomes a diffusion barrier to oxygen (O_2) delivery from the RBC core to the tissues, and to the scavenging of nitric oxide (NO) by the RBCs[5,6]. In addition, the production of NO can also be modulated by the dynamic variations of the CFL width[7,8]. Therefore, the roles of the CFL in both gas transport and the regulation of homeostasis in microcirculation need to be fully ascertained to better understand blood flow in microcirculation. Recent studies have focused on bridging the hemodynamics and gas transport functions of the CFL in the microcirculation[9-12]. Furthermore, a separate set of studies has also investigated how the pathological elevation in RBC aggregation modulates CFL formation and its effect on O_2 and NO bioavailability in tissues[13,14].

The roles of the CFL become more significant in microcirculation where the relative size of the CFL width to the vessel diameter is prominent. This necessitates an effective approach of quantifying the CFL in *in vivo* blood flow. Particularly, image acquisition and image analysis are the two key components determining the accuracy of CFL width measurement. Successful visualization of tissue blood flow should be preceded by an appropriate surgical preparation of the animal model. Additionally, a proper image analysis technique is needed to overcome the limitations of conventional manual measurements that are mostly induced by human errors[15,16]. With advancements in optical instrumentation and computing power for digital image processing, it is now possible to achieve a more accurate and consistent measurement of the CFL width[17-19]. Nonetheless, the accuracy of these measurements, being image-based, still ultimately depends on the quality of the images.

Therefore, this study explores the factors influencing the measurement of the *in vivo* CFL width. We focused particularly on demonstrating the surgical preparation and digital image analysis for measurements of the CFL width in arterioles of the rat cremaster muscle.

Protocol

This study is in accordance with the National University of Singapore Institutional Animal Care and Use Committee (approved protocol no. R15-0225).

1. Surgical Preparation of the Animal Model

1. **Vessel cannulations**
    1. Anesthetize a male Sprague-Dawley rats (6 - 7 weeks old) weighing (203 ± 20) g with ketamine (37.5 mg/ml) and xylazine (5 mg/ml) cocktail through intraperitoneal (i.p.) injection (2 ml/kg). Do not recap the needle or remove it from the syringe after the injection.
    2. Once the animal has been anesthetized (confirmed by toe pinching), place it on a heating pad to maintain its body temperature at 37 °C. Gently shave the hair on the scapulae, anterior cervix, lower abdomen, medial hind leg and scrotal sac. Gently restrain the legs using adhesive paper tapes.
    3. Perform all surgical procedures using microdissection scissors and angled forceps while viewing through a stereomicroscope. Place all sharp surgical tools on a puncture-resistant tray to prevent injury during the surgery.
    4. Scrub all surgical sites 3 times with alternating iodine and 70% alcohol before performing the incision. Flush all catheters with 30 IU/ml heparin-saline solution.
    5. Make a 1 - 1.5 cm midline skin incision on the scapulae using a pair of surgical scissors over the right jugular vein. Separate the fascia by blunt dissection to expose the jugular vein and cannulate it with a polyethylene tube (PE-50) filled with heparin-saline using 5-0 silk sutures. Infuse supplemental anesthesia when necessary (1/3 to 1/2 of initial dosage, intravenous (i.v.)) throughout the course of surgery and experiment.
    6. Perform tracheostomy to maintain airway patency. Make a 1 - 1.5 cm incision in the anterior cervical area. Cannulate the trachea using a polyethylene tube (PE-205) with 2-0 silk sutures to secure the catheter in place.
    7. Monitor blood pressure through cannulation at the femoral artery. Make a 1 - 1.5 cm incision at the left medial surface of the hind leg. Separate the femoral artery by blunt dissection. Cannulate the femoral artery with a polyethylene tube (PE-10) filled with heparin-saline using 5-0 silk sutures.

2. **Cremaster Muscle Preparation and Flow Visualization**
    1. Insert a 5-0 silk suture through the apex of the scrotal sac to extend it. Make an incision along the ventral surface of the scrotal sac. Regularly apply warm isotonic solution (37 °C; pH 7.4) to the exposed muscle.
    2. Remove surrounding connective tissues carefully and thoroughly using a cotton-tipped applicator.
    3. Insert a 5-0 silk suture through the apex of the cremaster muscle. Cut the suture into two pieces of equal length and tie a knot on each side. Cut the muscle between the two knots and stretch it onto a customized transparent Plexiglas platform by gently pulling the suture. Fix the end of the suture onto the platform with blue tack.
    NOTE: Thorough removal of surrounding connective tissues is crucial in obtaining optimum image contrast.
    4. Repeat step 1.2.3 until 5 to 6 fixations are made. Carefully remove the cremaster muscle from the epididymis using high temperature cautery. Superfuse warm isotonic solution to the exposed muscle to prevent dehydration of the tissue.
        1. Surround the cremaster muscle with folded pieces of gauze. Cover the exposed muscle with a polyvinyl film. The gauze pieces with the film form a shallow basin to hold warm isotonic solution for the water-immersion microscope objective (**Figure 1A**).
    5. Transfer the animal onto the animal stage of an intravital microscope (**Figure 1C**). Connect the arterial cannulation to a physiological data-acquisition system for continuous pressure monitoring (**Figure 1E**).
    6. Maintain the muscle temperature at 35 °C with a heating element attached beneath the animal platform (**Figure 1B**). Place a temperature probe beside the muscle to provide negative feedback to the power controller of the heating element (**Figure 1D**).
    7. Leave the animal on the stage for 15 min to equilibrate with the environment.
    8. Visualize blood flow under an intravital microscope with a 40X water-immersion objective and a long working condenser.
    9. Choose an unbranched arteriole (< 60 µm) based on a clear image focus and contrast between the RBC core, CFL and vessel walls, in order to focus the microscope on the diametric plane of the blood vessel. Rotate the camera mounted onto the microscope to align the vessel wall vertically.
    10. Record the blood flow using a high-speed video camera at a frame rate of 3,000/sec for 1 sec. Save the recorded video as uncompressed 8-bit grayscale AVI format to preserve the image quality.
    NOTE: A minimum recording frame rate of 3,000 frames/sec is recommended to ensure that the CFL measurement can be performed at least once per RBC under physiological arteriolar flow conditions.
    11. Use a blue filter with peak transmission at a wavelength of 394 nm and spectral bandpass at 310 - 510 nm to enhance the contrast between the RBCs and plasma.
    NOTE: Ensure that the light spectrum passing through the blue filter from the microscopic light source (100 W halogen lamp) is of low light intensity to prevent any potential tissue damage.
    12. At the end of the experiment, euthanize the animal with an overdose of pentobarbital sodium.

2. Image Analysis

1. **Preprocessing for the CFL width measurement**
    1. Open MATLAB and run the 'CFL_pre.m' file. (This and other MATLAB files can be found in the Supplemental MATLAB Archive.)
    2. Click 'Open file' to select the video file to analyze.

3. Adjust the 'Rotation' slider to align the vessel walls vertically.
   NOTE: Users can display the assisting grid lines for the vessel alignment by selecting the 'Grid On' radio button, and adjust the zoom level of the image by sliding the 'Zoom' slider.
4. Click the 'Confirm Editing' button to confirm the vessel alignment.
5. Click the 'Set ROI to crop' button to define the region of interest (ROI). The aligned image will be displayed in a pop-up window. Adjust the rectangular objective on the image, and double click to confirm the ROI. Skip this step if the cropping of image is not required.
   NOTE: Only include a single vessel in the ROI to analyze the CFL width from the vessel. Click the 'Reset Image' button to restore the image to its original form, if necessary.
6. Click the 'Extract Images' button to extract all edited video frames into consecutive bit map images (8-bit grayscale 'bmp' format). The extracted images can be found in the folder with the same name as the selected video file.

2. **Measurement of CFL width**
   1. Open MATLAB and run the 'CFL_measure.m' file.
   2. Click 'Select Folder' to select the folder containing the extracted images.
   3. Click on the folder containing the images and click 'Select Folder'. The first image frame in the folder will be loaded and shown in the 'Grayscale image' panel, along with its gray intensity histogram in the 'Image Histogram' panel.
   4. Select the desired image frame from the list box to perform the analysis, otherwise the first image frame will be selected.
   5. Click 'Find Vessel Walls' to identify the inner vessel wall in the image, which is determined at the location where the light intensity profile peak transits from dark to light over two pixels.
   6. Check 'Median Filter' to apply a median filter to the image to reduce the 'salt and pepper' noise.
   7. Check 'Auto Contrast' to adjust the image intensities digitally to enhance the image contrast.
   8. Select a thresholding algorithm in the list box which automatically determines a thresholding value (τ) that divides the gray levels into two classes — white pixels with gray levels above τ (CFL), and black pixels with gray levels below τ (RBC core).
      NOTE: As an alternative method, use manual thresholding if none of automated-thresholding algorithm provides an appropriate image thresholding. Click on the 'Manual' radio button and adjust the slider to define the manual thresholding value.
   9. To measure the spatial variation of the CFL widths, enter the pixel resolution in the 'Pixel Resolution' box (the resolution with this experimental setup was 0.42 µm/pixel).
   10. Click the 'Calculate' button to obtain the spatial variation of the CFL widths. Click 'Export .csv' to export the CFL width data in a tabulated format.
   11. To measure the temporal variation of the CFL widths at a specific analysis line along the vessel, click on the 'Temporal Variation' radio button and enter the frame rate information (the frame rate used in this experimental setup was 3,000 frames/sec).
   12. Enter the first frame and last frame of the images for the analysis in the 'Start Frame' and 'Last Frame' boxes, respectively.
   13. Select the position of the analysis line along the vessel by sliding the 'Analysis Line' slide bar. Confirm the position of the analysis line, which is illustrated on both the 'Grayscale image' and 'Binary image'.
   14. Click 'Calculate' to obtain the temporal variation of the CFL widths. Click 'Export .csv' to export the CFL width data in a tabulated format.

Representative Results

The visualization of the CFL *in vivo* is largely dependent on the surgical preparations of the animal. Excessive blood loss or extended surgery duration may subject the animal to shock and blood flow aberrations. Maintenance of tissue temperature using a heating pad as well as a customized platform during the surgery and experiment is also crucial for maintaining the physiological conditions of the rat. By using a 100 W halogen lamp in the microscope system, no discernible tissue damage was observed even at the end of the experiment.

Figure 2A shows a typical RBC flow through an unbranched arteriole in the rat cremaster muscle, where the CFL can be observed between the RBC core and the inner vessel wall (**Figure 2C**). A good contrast between these components during the experiment is critical for ensuring the accuracy of CFL width measurements. The initial phase of the image analysis involves the detection of the inner vessel wall. By acquiring the light intensity profile along the analysis line perpendicular to the vessel, the location is approximated at the peak that transits from dark to light over two pixels (**Figure 2B**).

As RBCs and CFL possess different light transmittance, the difference in gray levels can be subdivided into two classes (binary image). However, the identification of an accurate threshold value between the two peaks in the image histogram may be restricted by poor image quality and contrast (**Figure 3A**). To improve the contrast between the RBCs and CFL, a blue filter can be used (**Figure 3B**). This is also evident in **Figure 4**, in which the boundaries of the RBC core can be more accurately identified with the use of a blue filter. Furthermore, the selection of thresholding algorithm[20-23] can also influence the measurement of the CFL width (**Figure 4**). It is apparent in **Figure 4A** that different thresholding algorithms resulted in different RBC core boundary identified, which could in turn lead to erroneous CFL measurements. To better illustrate the influence of the thresholding algorithm on the CFL width measurement in **Figure 4B**, the spatial profiles for the CFL widths obtained using different thresholding algorithms are shown in **Figure 5** and summarized in **Table 1**.

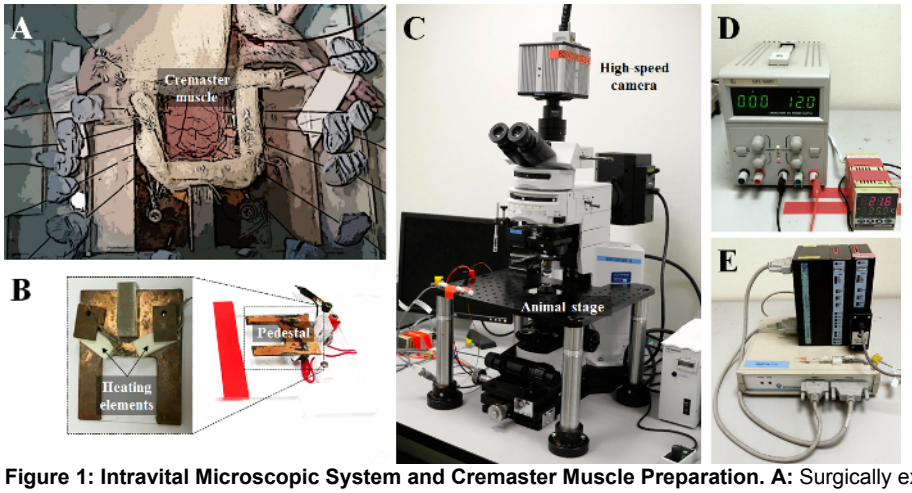

Figure 1: Intravital Microscopic System and Cremaster Muscle Preparation. A: Surgically exteriorized rat cremaster muscle. **B:** Customized platform with heating elements for placing the cremaster muscle and maintaining its temperature at 35 °C. **C:** Microscopic system with customized animal stage and high-speed camera for the visualization of microcirculatory blood flows in the cremaster muscle. **D:** Negative feedback temperature controller and power supply. **E:** Physiological data-acquisition system for continuous pressure monitoring. Please click here to view a larger version of this figure.

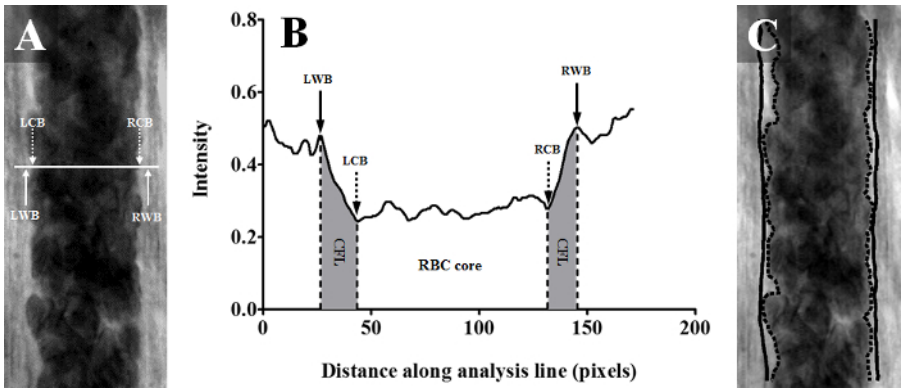

Figure 2: Image Processing for Determination of Vessel Wall Position and CFL Width. A: Typical grayscale image of RBC flow in an arteriole (vessel diameter = 52 µm). **B:** Light intensity profile along the analysis line (solid line in panel **A**). **C:** Representative result of CFL measurement along the vessel. The solid and dashed arrows indicate the inner vessel wall and outer edge of the RBC core, respectively. (LWB & RWB: left and right vessel wall boundary, LCB & RCB: left and right RBC core boundary) Please click here to view a larger version of this figure.

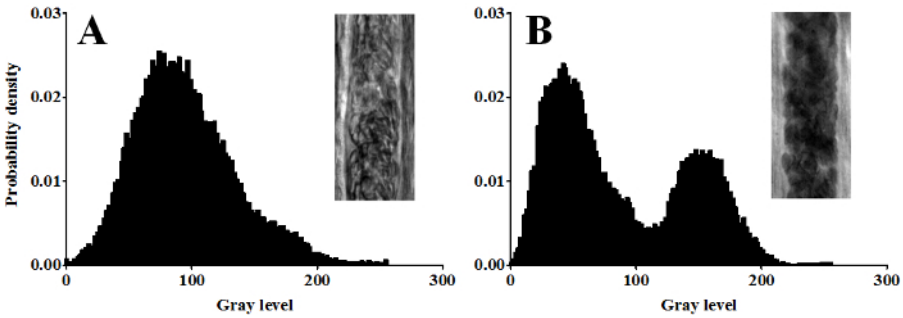

Figure 3: Image Contrast Enhancement with an Optical Blue Filter. Image histogram of the grayscale images obtained without (**A**) and with blue filter (**B**). Please click here to view a larger version of this figure.

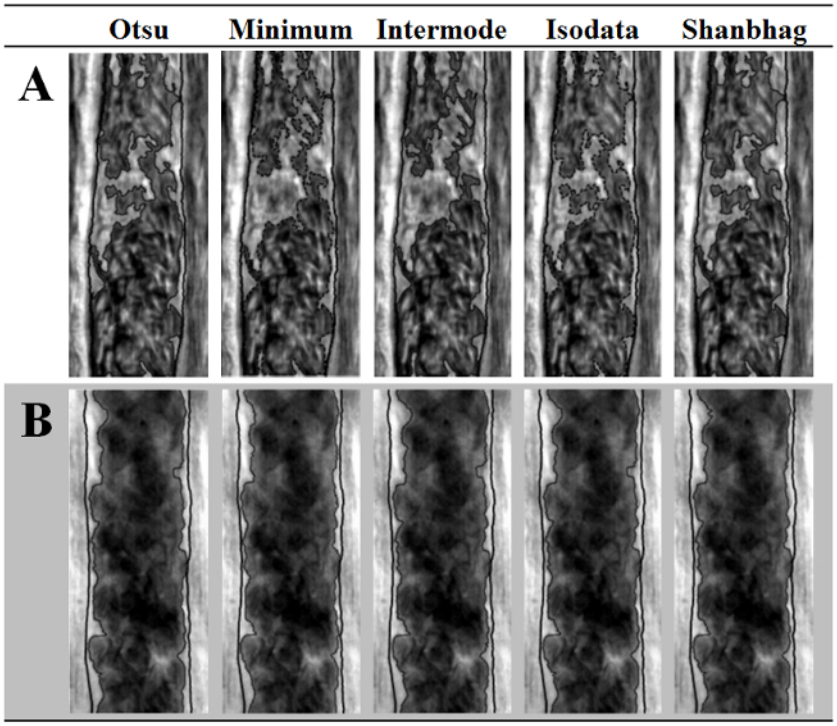

Figure 4: RBC Core Width Determined using Five Different Thresholding Algorithms. Boundaries of RBC core and vessel wall superimposed on grayscale images in **Figure 3**. (Top row (**A**): without blue filter, bottom row (**B**): with blue filter) using (from left to right) the Otsu's method, minimum method, intermode method, iterative selection method (Isodata) and fuzzy entropic thresholding (Shanbhag). The solid and dashed lines indicate the inner vessel wall and outer edge of the RBC core, respectively. Please click here to view a larger version of this figure.

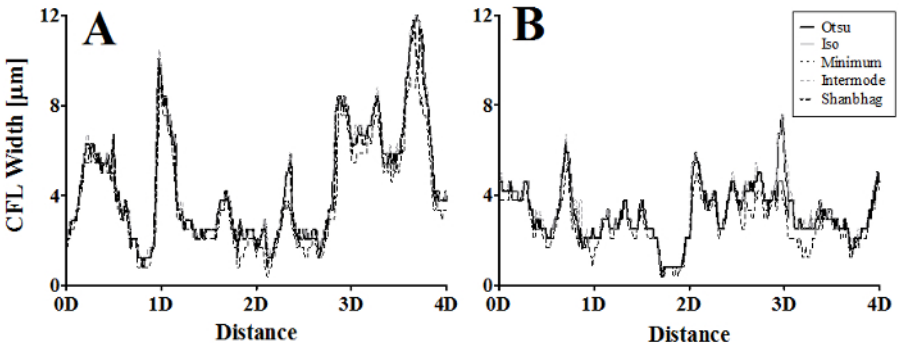

Figure 5: Spatial Variation of CFL Width. CFL widths corresponding to **Figure 4B** along the left (**A**) and right (**B**) vessel walls, respectively. (D: distance in vessel diameter) Please click here to view a larger version of this figure.

Thresholding algorithm	Threshold grayscale value (τ)	Optical Filter	CFL width (μm)	
			Left	Right
Otsu	120	Central wavelength = 394 nm	4.58 ± 2.61	3.24 ± 1.24†
Minimum	138		3.86 ± 2.29*	2.72 ± 1.03*,†
Intermode	116		4.70 ± 2.65	3.37 ± 1.28†
Isodata	120	Bandpass = 310-510 nm	4.58 ± 2.61	3.24 ± 1.24†
Shanbhag	123		4.44 ± 2.61	3.11 ± 1.10†

Table 1: Threshold Values and CFL Width Data in Figure 5. * $p < 0.001$: significant difference from Otsu's method. † $p < 0.001$: significant difference from left. Statistical analyses were performed using two-tailed unpaired t-tests.

Discussion

The measurement of CFL width is essential for a better understanding of the hemodynamics in the microcirculation. In particular, the measurement of CFL widths has been performed in mesenteric[6], spinotrapezius[24] and cerebral[25] microcirculations. Conventional measurement of *in vivo* CFL widths was restricted to estimations by manual inspection of the recorded video frames. The manual measurements required

the averaging of several successive video frames before visually identifying the boundaries of the RBC core and vessel walls[15,16]. In another study, fluorescein isothiocyanate (FITC)-labelled RBCs and rhodamine-B isothiocynate (RITC) labelled plasma were used to determine the mean CFL widths in cat cerebral microvessels[25]. These previous measurement methods are very time consuming and require additional steps for the fluorescent labelling, which limits the spatial and temporal resolution of the CFL width measurement. In contrast, by coupling high-speed camera recordings to an effective image segmentation and analysis, the technique demonstrated here permits the quantification of spatiotemporal variations of the CFL with a spatial resolution (0.42 µm) of an order smaller than the size of a RBC and a temporal resolution of 1/3,000 sec.

Proper surgical preparation of the cremaster muscle is critical in determining the accuracy of the CFL width measurements. In particular, thorough removal of adjacent connective tissues is essential to ensure a good focus of the arterioles in the cremaster muscle. In addition, the temporal and spatial resolution of the measurement is dependent on the microscope and camera specifications. While a higher magnification objective may enhance the spatial resolution, it reduces the field of view, which in turn limits the obtainable vessel length for quantifying the spatial variation of the CFL width. Therefore, the microscopic configurations can be modified according to the specific application of the technique.

Image segmentation is another important factor for the accuracy of the CFL width measurement. Amongst the various techniques developed, image thresholding based on gray level histogram provides a simple and effective approach for image segmentation and analysis. Accordingly, foreground objects are extracted from the background based on the difference in their gray levels. In the ideal case, the image histogram will be bimodal and a threshold value at the bottom of the valley is trivial. However, *in vivo* experimental images do not always exhibit such grayscale level profiles. Our results have shown how the image quality and contrast can influence the image segmentation process. The use of an optical blue filter significantly enhanced the contrast between the RBCs and the plasma in an arteriole (**Figure 3**), and it seems to be essential when applying the histogram-based thresholding for the CFL width measurement regardless of the algorithms (**Figure 4**). This results in a distinct bimodal image histogram, which allows one to identify the threshold value effectively. However, it should be noted that even with a bimodal histogram obtained from the *in vivo* images, an extremely unequal variance of two peaks (local maxima) and a wide valley (local minimum) of the histogram can still influence the threshold selection (**Table 1**). Therefore, the selection of an appropriate thresholding algorithm needs to be examined based on the image quality and users have to consider the limitations of each thresholding algorithm for the best suitability in quantifying CFL widths.

As the CFL widths are largely dependent on the flow conditions, continuous arterial pressure measurement throughout the course of the experiment is essential. In order to determine the local flow conditions, the pseudoshear rate of the blood flow can be computed by measuring the mean flow velocity in the blood vessel[5].

In summary, the protocols for the surgical preparation of a rat cremaster muscle and quantitative image analysis described here have been utilized to acquire quantitative information on the dynamic variation of the CFL widths *in vivo*. The primary challenges in ensuring the accuracy of the CFL width measurements include proper surgical preparation of the muscle and image segmentation, both of which have been addressed above. This technique can be readily adapted to other microcirculatory studies to investigate the hemorheological and hemodynamic aberrations in various physiological and pathological conditions. Consequently, these findings contribute to the future development of microvascular therapeutic approaches and clinical intervention.

Disclosures

The authors declare no competing financial interests.

Acknowledgements

This work was supported by National Medical Research Council (NMRC)/Cooperative Basic Research Grant (CBRG)/0078/2014.

References

1. Kim, S., Kong, R. L., Popel, A. S., Intaglietta, M., & Johnson, P. C. Temporal and spatial variations of cell-free layer width in arterioles. *Am J Physiol Heart Circ Physiol.* **293** (3), H1526-1535 (2007).
2. Ong, P. K., Namgung, B., Johnson, P. C., & Kim, S. Effect of erythrocyte aggregation and flow rate on cell-free layer formation in arterioles. *Am J Physiol Heart Circ Physiol.* **298** (6), H1870-1878 (2010).
3. Namgung, B., & Kim, S. Effect of uneven red cell influx on formation of cell-free layer in small venules. *Microvasc Res.* **92** 19-24 (2014).
4. Goldsmith, H. L. The Microcirculatory Society Eugene M. Landis Award Lecture. The Microrheology of Human-Blood. *Microvasc Res.* **31** (2), 121-142 (1986).
5. Buerk, D. G. Can We Model Nitric Oxide Biotransport? A Survey of Mathematical Models for a Simple Diatomic Molecule with Surprisingly Complex Biological Activities. *Annu Rev Biomed Eng.* **3** (1), 109-143 (2001).
6. Tateishi, N., Suzuki, Y., Soutani, M., & Maeda, N. Flow dynamics of erythrocytes in microvessels of isolated rabbit mesentery: cell-free layer and flow resistance. *J Biomech.* **27** (9), 1119-1125 (1994).
7. Ong, P. K., Cho, S., Namgung, B., & Kim, S. Effects of cell-free layer formation on NO/O2 bioavailability in small arterioles. *Microvasc Res.* **83** (2), 168-177 (2012).
8. Ong, P. K., Jain, S., & Kim, S. Modulation of NO bioavailability by temporal variation of the cell-free layer width in small arterioles. *Ann Biomed Eng.* **39** (3), 1012-1023 (2011).
9. Park, S. W., Intaglietta, M., & Tartakovsky, D. M. Impact of stochastic fluctuations in the cell free layer on nitric oxide bioavailability. *Front Comput Neurosci.* **9** 131 (2015).
10. Ng, Y. C., Namgung, B., & Kim, S. Two-dimensional transient model for prediction of arteriolar NO/O2 modulation by spatiotemporal variations in cell-free layer width. *Microvasc Res.* **97** 88-97 (2015).
11. Sriram, K. *et al.* The effect of small changes in hematocrit on nitric oxide transport in arterioles. *Antioxid Redox Sign.* **14** (2), 175-185 (2011).

12. Hightower, C. M. *et al.* Integration of cardiovascular regulation by the blood/endothelium cell-free layer. *Wiley Interdiscip Rev Syst Biol Med.* **3** (4), 458-470 (2011).
13. Ng, Y. C., Namgung, B., Leo, H. L., & Kim, S. Erythrocyte aggregation may promote uneven spatial distribution of NO/O in the downstream vessel of arteriolar bifurcations. *J Biomech.* (2015).
14. Ong, P. K., Jain, S., & Kim, S. Temporal variations of the cell-free layer width may enhance NO bioavailability in small arterioles: Effects of erythrocyte aggregation. *Microvasc Res.* **81** (3), 303-312 (2011).
15. Maeda, N. Erythrocyte rheology in microcirculation. *Jpn J Physiol.* **46** (1), 1-14, retrieved from http://www.ncbi.nlm.nih.gov/pubmed/8743714 (1996).
16. Soutani, M., Suzuki, Y., Tateishi, N., & Maeda, N. Quantitative Evaluation of Flow Dynamics of Erythrocytes in Microvessels - Influence of Erythrocyte Aggregation, retrieved from http://ajpheart.physiology.org/content/268/5/H1959. *Am J Physiol Heart Circ Physiol.* **268** (5), H1959-H1965 (1995).
17. Kim, S., Kong, R. L., Popel, A. S., Intaglietta, M., & Johnson, P. C. A computer-based method for determination of the cell-free layer width in microcirculation. *Microcirculation.* **13** (3), 199-207 (2006).
18. Soutani, M., Suzuki, Y., Tateishi, N., & Maeda, N. Quantitative Evaluation of Flow Dynamics of Erythrocytes in Microvessels - Influence of Erythrocyte Aggregation. *Am J Physiol Heart Circ Physiol.* **268** (5), H1959-H1965 (1995).
19. Namgung, B. *et al.* A comparative study of histogram-based thresholding methods for the determination of cell-free layer width in small blood vessels. *Physiol Meas.* **31** (9), N61-70 (2010).
20. Ong, P. K. *et al.* An automated method for cell-free layer width determination in small arterioles. *Physiol Meas.* **32** (3), N1-12 (2011).
21. Otsu, N. A Threshold Selection Method from Gray-Level Histograms. *IEEE Trans. Syst., Man, Cybern.* **9** (1), 62-66 (1979).
22. Prewitt, J. M., & Mendelsohn, M. L. The analysis of cell images. *Ann N Y Acad Sci.* **128** (3), 1035-1053 (1966).
23. Ridler, T. W., & Calvard, S. Picture Thresholding Using an Iterative Selection Method. *IEEE Trans. Syst., Man, Cybern.* **8** (8), 630-632 (1978).
24. Shanbhag, A. G. Utilization of Information Measure as a Means of Image Thresholding. *Cvgip-Graph Model Im.* **56** (5), 414-419 (1994).
25. Bishop, J. J., Popel, A. S., Intaglietta, M., & Johnson, P. C. Effects of erythrocyte aggregation and venous network geometry on red blood cell axial migration. *Am J Physiol Heart Circ Physiol.* **281** (2), H939-950 (2001).
26. Yamaguchi, S., Yamakawa, T., & Niimi, H. Cell-free plasma layer in cerebral microvessels. *Biorheology.* **29** (2-3), 251-260 (1992).

